

Research Article

Open Access



Extended state observer-based fault-tolerant control for an unmanned surface vehicle under asynchronous injection and deception attacks

Haiwen Wang¹, Chun Liu¹, Xiao Huang¹, Yuxuan Zhong², Dong Qu³, Ron J. Patton⁴

¹School of Mechatronic Engineering and Automation, Shanghai University, Shanghai 200444, China.

²China Ship Development and Design Center, Wuhan 430064, Hubei, China.

³School of Future Technology, Shanghai University, Shanghai 200444, China.

⁴School of Engineering, University of Hull, Hull HU6 7RX, UK.

Correspondence to: Prof. Chun Liu, School of Mechatronic Engineering and Automation, Shanghai University, No. 99, Shangda Road, Baoshan District, Shanghai 200444, China. E-mail: Chun Liu@shu.edu.cn

How to cite this article: Wang H, Liu C, Huang X, Zhong Y, Qu D, Patton RJ. Extended state observer-based fault-tolerant control for an unmanned surface vehicle under asynchronous injection and deception attacks. *Complex Eng Syst* 2024;4:13. <http://dx.doi.org/10.20517/ces.2024.19>

Received: 23 Apr 2024 **First Decision:** 21 Jun 2024 **Revised:** 2 Jul 2024 **Accepted:** 18 Jul 2024 **Published:** 24 Jul 2024

Academic Editor: Hamid Reza Karimi **Copy Editor:** Fangling Lan **Production Editor:** Fangling Lan

Abstract

This paper explores the problem of fault-tolerant control concerning an underactuated unmanned surface vehicle affected by actuator faults and disturbances in the physical layer and multiple cyber threats (time-varying delays, injection attacks, and deception attacks) in the networked layer. Firstly, an extended state observer is designed to estimate the relative state and fault information by constructing the estimation error term based on the output information affected by injection attack and delay. Secondly, a novel fault-tolerant controller is designed to deal with random Bernoulli deception attacks and compensate for time-varying delay and actuator faults by using the estimated information and considering the probability dynamics of deception attacks. Assuming that dual-channel asynchronous independent injection and deception attacks occur on the sensor-to-observer and observer-to-controller channels. A sufficient condition for asymptotic stability of the unmanned surface vehicle is derived by using Lyapunov-Krasovskii functional within the co-design framework of fault estimation and fault-tolerant control, and ensured by eliminating the equality constraint. Finally, the efficacy of the proposed algorithm is assessed through simulations of the unmanned surface vehicle under two distinct scenarios: low forward speed and high forward speed.

Keywords: Extended state observer, fault-tolerant control, unmanned surface vehicle, injection attacks, deception attacks



© The Author(s) 2023. **Open Access** This article is licensed under a Creative Commons Attribution 4.0 International License (<https://creativecommons.org/licenses/by/4.0/>), which permits unrestricted use, sharing, adaptation, distribution and reproduction in any medium or format, for any purpose, even commercially, as long as you give appropriate credit to the original author(s) and the source, provide a link to the Creative Commons license, and indicate if changes were made.



1. INTRODUCTION

For the past few years, the relevant technology of unmanned surface vehicles (USVs) has undergone rapid advancements, garnering substantial attention across various fields including military operations^[1], ocean exploration^[2], and maritime monitoring^[3]. An overview of control methods for USVs can be seen^[4]. Notably, considerable attention has been devoted to the fault-tolerant control (FTC) of nonlinear steering controlled^[5], underactuated^[6], and fully actuated^[7] USVs. An active FTC method for the USV is discussed^[8], while^[9] provides insights into a passive FTC approach. More cutting-edge research on FTC can be seen^[10–12]. Consequently, further exploration of FTC strategies for USVs is imperative to bolster reliability and stability of the system.

Given the intricacies of the marine environment, numerous accidents, including sensor faults (dead fault, biased fault, and random drift) and actuator faults (stuck steering mechanism-type fault and noise-type fault) along with insufficient thrust due to external disturbances, are prone to occur during mission execution. The smooth movement of USVs hinges upon various factors such as environmental perception and attitude control. These physical threats not only degrade the overall performance of USVs but also pose the risk of severe accidents. Hence, the FTC issues of USVs under physical threats are now receiving considerable attention^[13–15]. An observer is constructed based on an intermediate variable and an FTC protocol is designed for a USV with actuator faults and partial transmission data loss^[15]. Specifically, the FTC of USVs under actuator faults^[16], sensor faults^[17], thruster faults^[18], actuator faults and disturbances^[19] is investigated. In the FTC research, the observer-based active FTC method stands as a prominent choice^[8,20,21]. This approach revolves around extracting fault information from the fault estimation (FE) and subsequently designing an FTC strategy based on the estimated information. However, prevailing observer-based FTC methods conventionally separate the front-end FE from the back-end FTC which complicates the research of USVs. Conversely, the co-design of FE and FTC not only mitigates complexity but also abbreviates fault response durations, rendering it more conducive for a USV to move in complex environments. Therefore, it is necessary to further explore the applicability of FE and FTC co-design framework within the realm of USVs.

In addition to the adverse effects stemming from the aforementioned physical threats, the advancement of USV intelligence is also accompanied by cyber risks. On the one hand, attacks in the networked layer damage the connectivity of transmission channels and the integrity of data, diminishing the reliability of the USV and potentially leading to the deviation from prescribed routes and loss of control. Therefore, when facing such malicious attacks as denial of service (DoS) attack, deception attack, injection attack, how to design a suitable FTC scheme to withstand the impact is crucial. A concise summary of cyber threats faced by USVs across different domains is provided, and a data protection scheme is presented^[22]. Under the framework of co-design, a distributed control method based on the distributed unknown input observer is adopted to solve the distributed security control problem of multiple USVs under aperiodic DoS attacks^[23]. An event-triggered communication scheme and an event-based switching control system are proposed to deal with both delayed and aperiodic DoS attacks^[24]. A new defense and tolerance technology is adopted to deal with malicious connection hybrid attacks in the networked layer and solve the distributed tracking control problem of multiple USVs^[25]. However, the predominant focus of current research lies in the FTC for USVs under periodic/aperiodic DoS attacks^[23,24,26]. Different from DoS attacks which lead to serious communication interruption, deception attacks and injection attacks compromise the integrity and confidentiality of transmitted data by manipulating them, which causes misoperation of USVs and brings substantial security risks. On the other hand, the presence of network-induced delay significantly influences the real-time efficacy of USV control instructions, which greatly limits the flexibility of the system when performing tasks requiring rapid response such as obstacle avoidance. An event-triggered control design method for multiple USVs constrained by communication delay and drive resources is proposed to solve the dynamic target tracking problem^[27]. A novel nonlinear networked predictive control approach, leveraging the discrete sliding mode framework, is introduced to address the trajectory tracking challenges encountered by USVs in the presence of

communication limitations, encompassing network delay, packet loss, and packet disorder^[28]. The dynamic nature and inherent uncertainty associated with network-induced delay exert a notable influence on control precision, which establishes it as one of the key factors in USV control research. Furthermore, apart from the types of cyber threats, it is pertinent to contemplate the location of their influence. Most cyber threats involved in the research are imposed on the controller-actuator channel^[13,26,29] or sensor-to-fault detection filter channel^[30,31], ignoring other cases, particularly the sensor-to-observer (SO) and observer-to-controller (OC) channels. In the case of SO and OC channels facing cyber threats, the control system receives imprecise estimated information, thereby causing incorrect fault response. Consequently, in scenarios where both SO and OC channels encounter cyber attacks and delays and the system is subjected to physical threats, the design of an observer-based FTC strategy is significant to safeguard the security and stability of a USV in complex environments.

The primary contributions of this paper are as follows. (1) In contrast to previous investigations of USVs focusing on the single side such as faults^[17,18] or cyber attacks^[31,32], this paper presents a more comprehensive analysis by considering the combined impact of multiple cyber-physical threats. Different from the independent design of FE and FTC, this paper deduces the co-design criteria of FE and FTC under the unified framework based on Lyapunov-Krasovskii functional, and eliminates equality constraints, which alleviates the dilemma of solving nonlinear matrix inequalities; and (2) Unlike the prevailing emphasis on deception attacks and injection attacks^[31-33], the complex case of dual-channel asynchronous injection and deception attacks is considered, with the attacks specifically aimed at SO and OC channels. The fault-tolerant controller devised in this paper diverges from conventional active FTC configurations predicated on pure estimation data^[21,34]. Instead, it integrates adversarial and benign scenario considerations. Leveraging damaged estimation information, it strengthens the resilience of the USV to multiple cyber threats, rendering it more practical.

2. PROBLEM FORMULATION

2.1. USV modeling

The movement challenges encountered by a USV on the horizontal plane are examined within this paper, with due attention given to disturbances arising from environmental factors. Emphasis is placed exclusively on the sway-yaw-roll motion pattern of USV, illustrated in [Figure 1](#), with the repercussions of the heave-surge-pitch motion treated as perturbations. The dynamic model representing the USV is given as follows:

$$\begin{cases} \dot{r}(t) = K_{vr}v(t)/T_r + \omega_\psi(t)/T_r + K_{ar}\delta(t)/T_r - r(t)/T_r \\ \dot{p}(t) = \omega_n^2 K_{ap}\delta(t) - 2\zeta\omega_n p(t) + \omega_n^2\omega_\phi(t) - \omega_n^2\phi(t) + \omega_n^2 K_{vp}v(t) \\ \dot{v}(t) = K_{av}\delta(t)/T_v - v(t)/T_v \\ \dot{\psi}(t) = r(t) \\ \dot{\phi}(t) = p(t) \end{cases} \quad (1)$$

where $r(t)$, $v(t)$, $p(t)$, $\phi(t)$, $\delta(t)$, and $\psi(t)$ represent the yaw velocity, sway velocity, roll velocity, roll angle, rudder angle, and heading angle, respectively. $\omega_\psi(t)$ and $\omega_\phi(t)$ signify the external disturbances influencing the heading and roll velocity channels due to wave-induced effects. ω_n and ζ stand for the undamped natural frequency and damping ratio, respectively. The channel gains are denoted by K_{ap} , K_{ar} , K_{vp} , K_{vr} , and K_{av} , while T_r and T_v represent the time constants. To simplify the analysis, it is assumed that the speed of the USV remains the same.

During the propulsion of USVs, occurrences of actuator faults, such as noise-type faults and stuck steering mechanism-type faults, are inevitable. Consequently, the USV subject to external disturbances and actuator faults is modeled as:

$$\begin{cases} \dot{x}(t) = Ax(t) + Bu(t) + E\omega(t) + Ff(t) \\ y(t) = Cx(t) \end{cases} \quad (2)$$

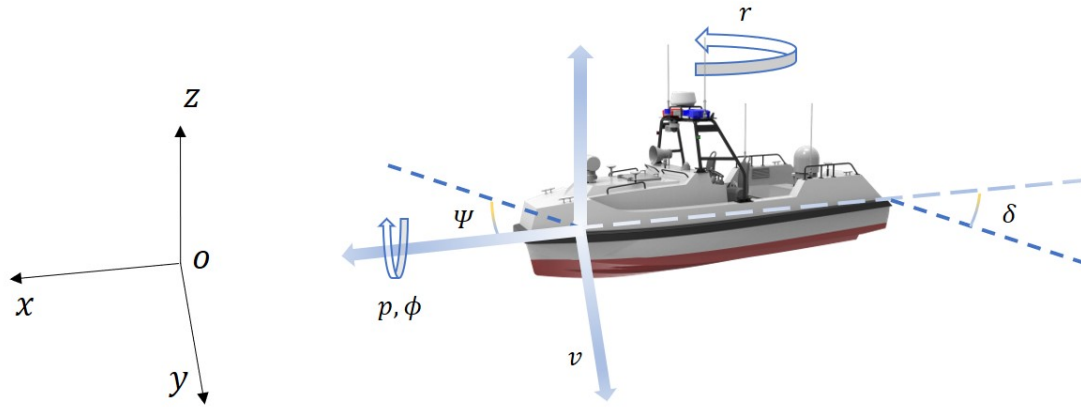


Figure 1. The sway-yaw-roll motion of USV illustrated in body-fixed coordinate frame.

where $x(t) = [v(t) r(t) \psi(t) p(t) \phi(t)]^T$ is the state of the USV. $u(t) = \delta(t)$ and $y(t)$ represent the input and output of the system, respectively. $\omega(t) = [\omega_\psi(t) \omega_\phi(t)]^T$ and $f(t)$ characterize the wave-induced disturbances and actuator faults. Matrices A, B, C, E and F are constant matrices, with A, B , and E derived from (1),

$$\begin{aligned}
 A &= \begin{bmatrix} -1/T_v & 0 & 0 & 0 & 0 \\ K_{vr}/T_r & -1/T_r & 0 & 0 & 0 \\ 0 & 1 & 0 & 0 & 0 \\ \omega_n^2 K_{vp} & 0 & 0 & -2\zeta\omega_n & -\omega_n^2 \\ 0 & 0 & 0 & 1 & 0 \end{bmatrix}, \\
 B &= \begin{bmatrix} K_{av}/T_v \\ K_{ar}/T_r \\ 0 \\ \omega_n^2 K_{ap} \\ 0 \end{bmatrix}, \quad E = \begin{bmatrix} 0 & 0 \\ 1/T_r & 0 \\ 0 & 0 \\ 0 & \omega_n^2 \\ 0 & 0 \end{bmatrix}.
 \end{aligned} \tag{3}$$

2.2. Asynchronous injection and deception attacks modeling

Concerning threats in the networked layer, considerable focus has been directed toward assessing the combined impact of network-induced delays, as well as asynchronous injection and deception attacks targeting transmitted signals across SO and OC channels, as portrayed in Figure 2.

Under the joint impact of time-varying delays and injection attacks, the output signal $y(t)$ transmitted on the SO channel is transformed into the following form,

$$\bar{y}(t) = y(t - \beta(t)) + \alpha y(t - \beta(t)) = \bar{\alpha} y(t - \beta(t)) \tag{4}$$

where $\bar{y}(t)$ indicates the affected output signal, and $\beta(t)$ represents the time-varying delay caused by network transmission process. The scaling factor α denotes the attack amplitude.

In intricate maritime settings, direct acquisition of the state information of the USV is unfeasible owing to the prevalence of interferences such as magnetic fields and waves. Hence, an extended state observer is proposed to simultaneously estimate state and fault information. The extended state observer is constructed as follows:

$$\begin{cases} \dot{\hat{x}}(t) = A\hat{x}(t) + Bu(t) + F\hat{f}(t) - L(\bar{y}(t) - \hat{y}(t)) \\ \hat{y}(t) = C\hat{x}(t) \\ \dot{\hat{f}}(t) = Q(\bar{y}(t) - \hat{y}(t)) \end{cases} \tag{5}$$

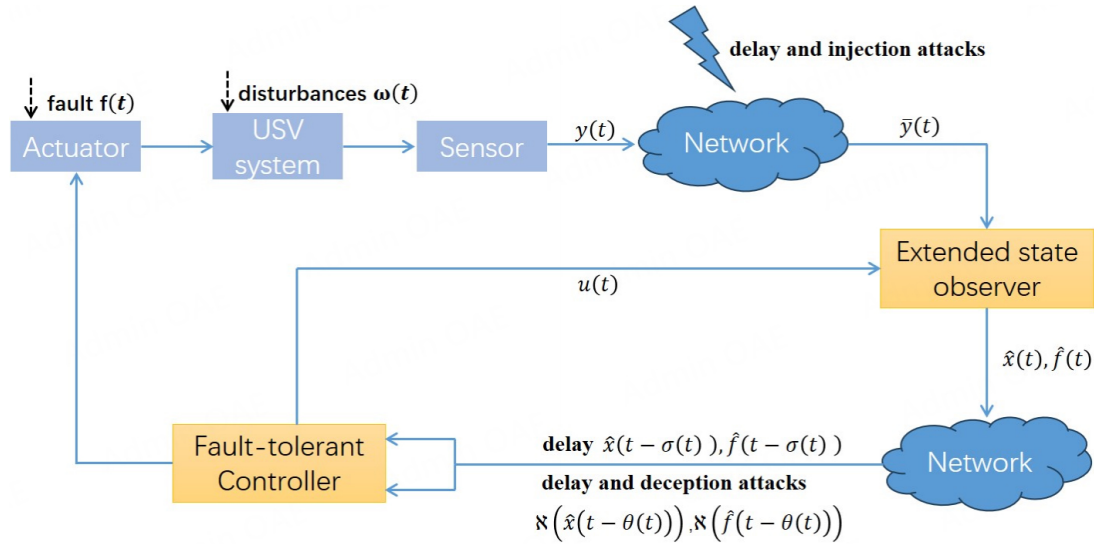


Figure 2. Dual-channel time-varying delays and asynchronous injection and deception attacks

where $\hat{x}(t)$ and $\hat{f}(t)$ represent the estimation of state information and fault information, respectively, which are transmitted to the fault-tolerant controller through OC channel. L and Q both are gain matrices to be determined.

In the context of deception attacks occurring on the OC channel, a stochastic variable denoted as $\rho(t)$ is introduced to delineate the probability associated with attack occurrences. The stochastic variable $\rho(t)$ is governed by the Bernoulli distribution and embodies the mathematical expectation formulated as follows:

$$\Pr(\rho(t) = 1) = \mathbb{E}\{\rho(t)\} = \bar{\rho}, \mathbb{E}\{(\rho(t) - \bar{\rho})^2\} = \bar{\rho}(1 - \bar{\rho}), \bar{\rho} \in [0, 1] \tag{6}$$

In addition to deception attacks, the existence of time-varying delays is also taken into account within the OC channel. When the estimated information $\hat{x}(t)$ and $\hat{f}(t)$ are transmitted through the OC channel to the fault-tolerant controller without being subjected to Bernoulli deception attacks, the received data are denoted as $\hat{x}(t - \sigma(t))$ and $\hat{f}(t - \sigma(t))$, respectively. Conversely, in the event of attacks, the data integrity is damaged, resulting in post-attack signals represented as $\aleph(\hat{x}(t - \theta(t)))$ and $\aleph(\hat{f}(t - \theta(t)))$. Both $\sigma(t)$ and $\theta(t)$ represent the time-varying delay on the OC channel.

Remark 1: The injection attacks on the SO channel and the deception attacks on the OC channel give rise to an asynchronous independent attacks phenomenon attributed to varying delays across channels. The disparity in delays and attack modalities poses challenges to the investigation of the controllability and reliability of the USV. Concerning the injection attack on the SO channel, it injects the attack signal by combining with the state information, which is more targeted and elusive than the attack that directly injects irrelevant information. In addition, in contrast to other researches focusing on Bernoulli deception attacks on channels^[35,36], no analogous constraint is imposed on the attacks.

Assumption 1:^[5,6,37] The time-varying delays occurring on either SO or OC channels have known upper bounds, i.e., $\beta(t) \in [0, \beta_M]$, $\sigma(t) \in [0, \sigma_M]$, $\theta(t) \in [0, \theta_M]$. In addition, both the derivative of the fault vector $\dot{f}(t)$ and the disturbance vector have an unknown upper bound, i.e., $\|\dot{f}(t)\| \leq \bar{f}$, $\bar{f} > 0$, $\|\omega(t)\| \leq \bar{\omega}$, $\bar{\omega} > 0$.

Assumption 2:^[24] The system matrix C^T satisfies full column rank.

Lemma 1:^[37] For the provided matrix $C^T \in \mathbb{R}^{n \times l}$ and positive definite matrix $W \in \mathbb{R}^{n \times n}$, there is a matrix $N \in \mathbb{R}^{l \times l}$ such that $WC^T = C^TN$ if and only if

$$W = J^T \begin{bmatrix} W_{11} & 0 \\ 0 & W_{22} \end{bmatrix} J \quad (7)$$

where $W_{11} \in \mathbb{R}^{l \times l}$, $W_{22} \in \mathbb{R}^{(n-l) \times (n-l)}$, and J is an orthogonal matrix.

Control objective: The main purpose is to design a fault-tolerant controller $u(t)$ within the FE and FTC co-design framework that enables the USV system (2) to achieve asymptotic stability under multiple cyber-physical threats such as disturbances, actuator faults, time-varying delays, injection attacks, and deception attacks.

3. MAIN RESULTS

In this section, the $u(t)$ is designed using the information estimated by the extended state observer. A sufficient condition for asymptotic stability of the USV system (2) is derived under the framework of FE and FTC co-design, and a method to eliminate the equality constraints is proposed to solve the unknown gain matrix to ensure the sufficient condition.

The state estimation error and FE error are respectively defined as $e_x = \hat{x}(t) - x(t)$, $e_f = \hat{f}(t) - f(t)$. The dynamics of the estimation errors are deduced by using (2) and (5) as follows:

$$\begin{cases} \dot{e}_x(t) = Ae_x(t) + Fe_f(t) - E\omega(t) + \bar{\alpha}L Ce_x(t - \beta(t)) - \bar{\alpha}L C\hat{x}(t - \beta(t)) + LC\hat{x}(t) \\ \dot{e}_f(t) = -\bar{\alpha}Q Ce_x(t - \beta(t)) + \bar{\alpha}Q C\hat{x}(t - \beta(t)) - Q C\hat{x}(t) - \dot{f}(t) \end{cases} \quad (8)$$

When time-varying delays and Bernoulli deception attacks exist within the OC channel, the state estimation information $\hat{x}(t)$ and FE information $\hat{f}(t)$ are utilized to construct the fault-tolerant controller $u(t)$ for the USV system (2), formulated as follows:

$$\begin{aligned} u(t) = & (1 - \rho(t)) K\hat{x}(t - \sigma(t)) + \rho(t) K\aleph(\hat{x}(t - \theta(t))) \\ & - (1 - \rho(t)) G\hat{f}(t - \sigma(t)) - \rho(t) G\aleph(\hat{f}(t - \theta(t))) \end{aligned}$$

In combination with (5), (8), and (9), the augmented system is constructed as follows:

$$\begin{aligned} \dot{\xi}(t) = & \hat{A}\xi(t) + \hat{C}\xi(t - \beta(t)) + (1 - \rho(t))\hat{B}M\xi(t - \sigma(t)) \\ & + \rho(t)\hat{B}\aleph(M\xi(t - \theta(t))) + \hat{E}\varpi(t) \end{aligned} \quad (9)$$

where $\xi(t) = [e_x^T(t) \ e_f^T(t) \ \hat{x}^T(t) \ \hat{f}^T(t)]^T$, and $\varpi(t) = [\omega^T(t) \ \dot{f}^T(t)]^T$ are the augmented vectors. $\hat{A} =$

$$\begin{bmatrix} A & F & LC & 0 \\ 0 & 0 & -QC & 0 \\ 0 & 0 & A + LC & F \\ 0 & 0 & -QC & 0 \end{bmatrix}, \hat{B} = \begin{bmatrix} 0 & 0 \\ 0 & 0 \\ BK & -BG \\ 0 & 0 \end{bmatrix}, M = \begin{bmatrix} 0 & 0 & I & 0 \\ 0 & 0 & 0 & I \end{bmatrix}, \hat{C} = \begin{bmatrix} \bar{\alpha}LC & 0 & -\bar{\alpha}LC & 0 \\ -\bar{\alpha}QC & 0 & \bar{\alpha}QC & 0 \\ \bar{\alpha}LC & 0 & -\bar{\alpha}LC & 0 \\ -\bar{\alpha}QC & 0 & \bar{\alpha}QC & 0 \end{bmatrix}, \text{ and}$$

$$\hat{E} = \begin{bmatrix} -E & 0 \\ 0 & -I \\ 0 & 0 \\ 0 & 0 \end{bmatrix} \text{ are the augmented matrices.}$$

Given the positive parameter $\gamma > 0$, the asymptotic stability of the USV system (2) is equivalent to the augmented system (9) satisfying the following H_∞ performance index.

$$\mathbb{E}\left\{\int_0^t \xi^T(s)\xi(s)ds\right\} \leq \gamma^2 \mathbb{E}\left\{\int_0^t \varpi^T(s)\varpi(s)ds\right\} \tag{10}$$

Theorem 1: Given the known parameters $\beta_M, \sigma_M, \theta_M, \bar{\rho}, \gamma$, and matrices $\hat{A}, \hat{B}, \hat{C}, \hat{E}, M$, the augmented system (9) can achieve asymptotic stability under the zero initial condition with an H_∞ index γ , if there exist positive definite matrices P, Θ_i , and $\Psi_i (i = 1, 2, 3)$ satisfying the following matrix inequality:

$$\Omega(s) = \begin{bmatrix} \Omega_{11} & * & * & * \\ \Omega_{21} & \Omega_{22} & * & * \\ \Omega_{31} & 0 & \Omega_{33} & * \\ \Omega_{41} & 0 & 0 & \Omega_{44} \end{bmatrix} < 0 \tag{11}$$

where

$$\Omega_{11} = \begin{bmatrix} \Upsilon & * & * & * & * & * & * & * \\ \hat{C}^T P & 0 & * & * & * & * & * & * \\ 0 & 0 & -\Theta_1 & * & * & * & * & * \\ (1-\bar{\rho})M^T \hat{B}^T P & 0 & 0 & 0 & * & * & * & * \\ 0 & 0 & 0 & 0 & -\Theta_2 & * & * & * \\ 0 & 0 & 0 & 0 & 0 & -\Theta_3 & * & * \\ \bar{\rho} \hat{B}^T P & 0 & 0 & 0 & 0 & 0 & 0 & * \\ \hat{E}^T P & 0 & 0 & 0 & 0 & 0 & 0 & -\gamma^2 I \end{bmatrix}$$

$$\Upsilon = P\hat{A} + \hat{A}^T P + \Theta_1 + \Theta_2 + \Theta_3 + I, \Omega_{22} = \Omega_{33} = \Omega_{44} = \text{Diag}\{-P\Psi_1^{-1}P, -P\Psi_2^{-1}P, -P\Psi_3^{-1}P\}$$

$$\Omega_{21} = \begin{bmatrix} \beta_M P \\ \sigma_M P \\ \theta_M P \end{bmatrix} \begin{bmatrix} \hat{A} & \hat{C} & 0 & (1-\bar{\rho})\hat{B}M & 0 & 0 & \bar{\rho}\hat{B} & \hat{E} \end{bmatrix}, m = \sqrt{\bar{\rho}(1-\bar{\rho})}$$

$$\Omega_{31} = \begin{bmatrix} m\beta_M P \\ m\sigma_M P \\ m\theta_M P \end{bmatrix} \begin{bmatrix} 0 & 0 & 0 & \hat{B}M & 0 & 0 & -\hat{B} & 0 \end{bmatrix}, \Omega_{41} = \begin{bmatrix} P & 0 & -P & 0 & 0 & 0 & 0 & 0 \\ P & 0 & 0 & 0 & -P & 0 & 0 & 0 \\ P & 0 & 0 & 0 & 0 & -P & 0 & 0 \end{bmatrix}.$$

Proof: The Lyapunov-Krasovskii functional $V(t)$ is framed as $V(t) = V_1(t) + V_2(t) + V_3(t)$ with the following form

$$\begin{aligned} V_1(t) &= \xi^T(t)P\xi(t) \\ V_2(t) &= \int_{t-\beta_M}^t \xi^T(s)\Theta_1\xi(s)ds + \int_{t-\sigma_M}^t \xi^T(s)\Theta_2\xi(s)ds + \int_{t-\theta_M}^t \xi^T(s)\Theta_3\xi(s)ds \\ V_3(t) &= \beta_M \int_{-\beta_M}^0 \int_{t+v}^t \xi^T(z)\Psi_1\dot{\xi}(z)dzdv + \sigma_M \int_{-\sigma_M}^0 \int_{t+v}^t \xi^T(z)\Psi_2\dot{\xi}(z)dzdv \\ &\quad + \theta_M \int_{-\theta_M}^0 \int_{t+v}^t \xi^T(z)\Psi_3\dot{\xi}(z)dzdv \end{aligned} \tag{12}$$

Then, the $\mathbb{E}\{\dot{V}(t)\}$ can be formulated as $\mathbb{E}\{\dot{V}(t)\} = \mathbb{E}\{\dot{V}_1(t)\} + \mathbb{E}\{\dot{V}_2(t)\} + \mathbb{E}\{\dot{V}_3(t)\}$, as delineated by the

subsequent expressions.

$$\begin{aligned}
 \mathbb{E}\{\dot{V}_1(t)\} &= 2\xi^T(t)P\Xi \\
 \mathbb{E}\{\dot{V}_2(t)\} &= \xi^T(t) (\Theta_1 + \Theta_2 + \Theta_3) \xi(t) - \xi^T(t - \beta_M) \Theta_1 \xi(t - \beta_M) \\
 &\quad - \xi^T(t - \sigma_M) \Theta_2 \xi(t - \sigma_M) - \xi^T(t - \theta_M) \Theta_3 \xi(t - \theta_M) \\
 \mathbb{E}\{\dot{V}_3(t)\} &= -\beta_M \int_{t-\beta_M}^t \xi^T(s) \Psi_1 \dot{\xi}(s) ds - \sigma_M \int_{t-\sigma_M}^t \xi^T(s) \Psi_2 \dot{\xi}(s) ds \\
 &\quad - \theta_M \int_{t-\theta_M}^t \xi^T(s) \Psi_3 \dot{\xi}(s) ds + \mathbb{E}\{\xi^T(t) \Psi \dot{\xi}(t)\}
 \end{aligned} \tag{13}$$

where

$$\begin{aligned}
 \mathbb{E}\{\xi^T(t) \Psi \dot{\xi}(t)\} &= \mathbb{E}\{\Xi + (\bar{\rho} - \rho(t)) \Xi_1\}^T \Psi \{\Xi + (\bar{\rho} - \rho(t)) \Xi_1\} = \Xi^T \Psi \Xi + m^2 \Xi_1^T \Psi \Xi_1 \\
 \Xi &= \hat{A} \xi(t) + \hat{C} \xi(t - \beta(t)) + (1 - \bar{\rho}) \hat{B} M \xi(t - \sigma(t)) + \bar{\rho} \hat{B} \mathfrak{N}(M \xi(t - \theta(t))) + \hat{E} \varpi(t) \\
 \Xi_1 &= \hat{B} M \xi(t - \sigma(t)) - \hat{B} \mathfrak{N}(M \xi(t - \theta(t))), \Psi = \beta_M^2 \Psi_1 + \sigma_M^2 \Psi_2 + \theta_M^2 \Psi_3.
 \end{aligned}$$

From the Jensen inequality, the following inequalities hold

$$\begin{aligned}
 -\beta_M \int_{t-\beta_M}^t \xi^T(s) \Psi_1 \dot{\xi}(s) ds &\leq -[\xi(t) - \xi(t - \beta_M)]^T \Psi_1 [\xi(t) - \xi(t - \beta_M)] \\
 -\sigma_M \int_{t-\sigma_M}^t \xi^T(s) \Psi_2 \dot{\xi}(s) ds &\leq -[\xi(t) - \xi(t - \sigma_M)]^T \Psi_2 [\xi(t) - \xi(t - \sigma_M)] \\
 -\theta_M \int_{t-\theta_M}^t \xi^T(s) \Psi_3 \dot{\xi}(s) ds &\leq -[\xi(t) - \xi(t - \theta_M)]^T \Psi_3 [\xi(t) - \xi(t - \theta_M)]
 \end{aligned} \tag{14}$$

In order to ensure that the augmented system (9) satisfies H_∞ index (10), the following calculation is performed under the zero initial condition,

$$\begin{aligned}
 \mathbb{E}\left\{\int_0^t \xi^T(s) \xi(s) ds\right\} - \gamma^2 \mathbb{E}\left\{\int_0^t \varpi^T(s) \varpi(s) ds\right\} &= \mathbb{E}\left\{\int_0^t (\xi^T(s) \xi(s) - \gamma^2 \varpi^T(s) \varpi(s)) ds\right\} \\
 &\leq \int_0^t \mathbb{E}\{\xi^T(s) \xi(s) - \gamma^2 \varpi^T(s) \varpi(s) + \dot{V}(s)\} ds \leq 2\xi^T(t)P\Xi + \xi^T(t) (\Theta_1 + \Theta_2 + \Theta_3) \xi(t) \\
 &\quad - \xi^T(t - \beta_M) \Theta_1 \xi(t - \beta_M) - \xi^T(t - \sigma_M) \Theta_2 \xi(t - \sigma_M) + \Xi^T \Psi \Xi + \xi^T(t) \xi(t) \\
 &\quad + m^2 \Xi_1^T \Psi \Xi_1 - \xi^T(t - \theta_M) \Theta_3 \xi(t - \theta_M) - [\xi(t) - \xi(t - \beta_M)]^T \Psi_1 [\xi(t) - \xi(t - \beta_M)] \\
 &\quad - \gamma^2 \varpi^T(t) \varpi(t) - [\xi(t) - \xi(t - \sigma_M)]^T \Psi_2 [\xi(t) - \xi(t - \sigma_M)] \\
 &\quad - [\xi(t) - \xi(t - \theta_M)]^T \Psi_3 [\xi(t) - \xi(t - \theta_M)]
 \end{aligned} \tag{15}$$

The inequality (11) is a sufficient condition for $\mathbb{E}\{\dot{V}(t) + \xi^T(t) \xi(t) - \gamma^2 \varpi^T(t) \varpi(t)\} < 0$ with the definition of $s(t) = [\xi^T(t) \xi^T(t - \beta(t)) \xi^T(t - \beta_M) \xi^T(t - \sigma(t)) \xi^T(t - \sigma_M) \xi^T(t - \theta_M) \mathfrak{N}^T(M \xi(t - \theta(t))) \varpi^T(t)]^T$ through using the Schur complement in the inequality (15).

Remark 2: In formulating the aforementioned Lyapunov-Krasovskii functional $V(t)$, the parameters β_M , σ_M and θ_M signify the upper bounds of the corresponding channel delays to model worst-case scenarios. Thus, inequality (10) persists under the condition that the time-varying delays of the channels remain within the prescribed upper bounds in all cases.

The resolution of matrix inequalities (11) poses challenges in directly solving the unknown matrix parameters employing the linear matrix inequalities (LMI) technique, attributed to the inclusion of partial nonlinear terms. Consequently, a method is introduced in the following theorem to eliminate equality constraints,

thereby linearizing the nonlinear terms, and subsequently resolving multiple undetermined matrix parameters via a matrix inequality.

Theorem 2: Given the scalars $\beta_M, \sigma_M, \theta_M, \bar{\rho}, \gamma, \epsilon_i (i = 1, 2, 3, 4)$ and matrices $\hat{A}, \hat{B}, \hat{C}, \hat{E}$, after eliminating the equality constraint, the augmented system (9) achieves the H_∞ performance index (10) if there exist positive definite matrices $W, \tilde{\Theta}_i, \Psi_i (i = 1, 2, 3)$ and matrices $\tilde{Q}, \tilde{L}, \tilde{K}, G$ such that the following inequalities can be solved,

$$\tilde{\Omega}(s) = \begin{bmatrix} \tilde{\Omega}_{11} & * & * & * \\ \tilde{\Omega}_{21} & \tilde{\Omega}_{22} & * & * \\ \tilde{\Omega}_{31} & 0 & \tilde{\Omega}_{33} & * \\ \tilde{\Omega}_{41} & 0 & 0 & \tilde{\Omega}_{44} \end{bmatrix} < 0 \tag{16}$$

where

$$\tilde{\Omega}_{11} = \begin{bmatrix} \tilde{Y} & * & * & * & * & * & * & * \\ \tilde{C} & 0 & * & * & * & * & * & * \\ 0 & 0 & -\tilde{\Theta}_1 & * & * & * & * & * \\ (1-\bar{\rho})\tilde{B} & 0 & 0 & 0 & * & * & * & * \\ 0 & 0 & 0 & 0 & -\tilde{\Theta}_2 & * & * & * \\ 0 & 0 & 0 & 0 & 0 & -\tilde{\Theta}_3 & * & * \\ \bar{\rho}\tilde{B}_1 & 0 & 0 & 0 & 0 & 0 & 0 & * \\ \hat{E}^T & 0 & 0 & 0 & 0 & 0 & 0 & -\gamma^2 I \end{bmatrix}$$

$$\tilde{Y} = \tilde{A} + \tilde{A}^T + \tilde{\Theta}_1 + \tilde{\Theta}_2 + \tilde{\Theta}_3 + I, \tilde{\Omega}_{22} = \tilde{\Omega}_{33} = \tilde{\Omega}_{44} = \text{Diag} \{-\Psi_1^{-1}, -\Psi_2^{-1}, -\Psi_3^{-1}\}$$

$$\tilde{\Omega}_{21} = \begin{bmatrix} \beta_M \\ \sigma_M \\ \theta_M \end{bmatrix} \begin{bmatrix} \tilde{A} & \tilde{C}^T & 0 & (1-\bar{\rho})\tilde{B}^T & 0 & 0 & \bar{\rho}\tilde{B}_1^T & \hat{E} \end{bmatrix}$$

$$\tilde{\Omega}_{31} = \begin{bmatrix} m\beta_M \\ m\sigma_M \\ m\theta_M \end{bmatrix} \begin{bmatrix} 0 & 0 & 0 & \tilde{B}^T & 0 & 0 & -\tilde{B}_1^T & 0 \end{bmatrix}, \tilde{\Omega}_{41} = \begin{bmatrix} P^{-1} & 0 & -P^{-1} & 0 & 0 & 0 & 0 & 0 \\ P^{-1} & 0 & 0 & 0 & -P^{-1} & 0 & 0 & 0 \\ P^{-1} & 0 & 0 & 0 & 0 & 0 & -P^{-1} & 0 \end{bmatrix}$$

$$\tilde{A} = \hat{A}P^{-1} = \begin{bmatrix} \epsilon_1 AW & \epsilon_2 F & \epsilon_3 \tilde{L}^T C & 0 \\ 0 & 0 & -\epsilon_3 \tilde{Q}^T C & 0 \\ 0 & 0 & \epsilon_3 AW + \epsilon_3 \tilde{L}^T C & \epsilon_4 F \\ 0 & 0 & -\epsilon_3 \tilde{Q}^T C & 0 \end{bmatrix}, \tilde{B} = P^{-1}M^T \hat{B}^T = \begin{bmatrix} 0 & 0 & 0 & 0 \\ 0 & 0 & 0 & 0 \\ 0 & 0 & \epsilon_3 \tilde{K} B^T & 0 \\ 0 & 0 & -\epsilon_4 G^T B^T & 0 \end{bmatrix}$$

$$\tilde{B}_1 = P^{-1}\hat{B}^T = \begin{bmatrix} 0 & 0 & \epsilon_3 \tilde{K} B^T & 0 \\ 0 & 0 & -\epsilon_4 G^T B^T & 0 \end{bmatrix}, \tilde{\Theta}_i = P^{-1}\Theta_i P^{-1}, (i = 1, 2, 3)$$

$$\tilde{C} = P^{-1}\hat{C}^T = \begin{bmatrix} \epsilon_1 \tilde{\alpha} C^T \tilde{L} & -\epsilon_1 \tilde{\alpha} C^T \tilde{Q} & \epsilon_1 \tilde{\alpha} C^T \tilde{L} & -\epsilon_1 \tilde{\alpha} C^T \tilde{Q} \\ 0 & 0 & 0 & 0 \\ -\epsilon_1 \tilde{\alpha} C^T \tilde{L} & \epsilon_1 \tilde{\alpha} C^T \tilde{Q} & -\epsilon_1 \tilde{\alpha} C^T \tilde{L} & \epsilon_1 \tilde{\alpha} C^T \tilde{Q} \\ 0 & 0 & 0 & 0 \end{bmatrix}$$

$$P^{-1} = \begin{bmatrix} \epsilon_1 W & 0 & 0 & 0 \\ 0 & \epsilon_2 I & 0 & 0 \\ 0 & 0 & \epsilon_3 W & 0 \\ 0 & 0 & 0 & \epsilon_4 I \end{bmatrix}, P_1^{-1} = \begin{bmatrix} \epsilon_3 W & 0 \\ 0 & \epsilon_4 I \end{bmatrix}.$$

Proof: For the matrix $C^T \in \mathbb{R}^{n \times l}$ of the full column rank, there exist two orthogonal matrices $J \in \mathbb{R}^{n \times n}$ and $Y \in \mathbb{R}^{l \times l}$ such that

$$JC^TY = \begin{bmatrix} J_1 \\ J_2 \end{bmatrix} C^TY = \begin{bmatrix} \Delta \\ 0 \end{bmatrix} \quad (17)$$

where $J_1 \in \mathbb{R}^{l \times n}$, $J_2 \in \mathbb{R}^{(n-l) \times n}$, and $\Delta = \text{Diag}\{\sigma_1, \dots, \sigma_l\}$ for $\sigma_1, \dots, \sigma_l$ being nonzero singular values of C^T . Constructing the following matrix W ,

$$W = J^T \begin{bmatrix} W_{11} & 0 \\ 0 & W_{22} \end{bmatrix} J = J_1^T W_{11} J_1 + J_2^T W_{22} J_2 \quad (18)$$

where W_{11} and W_{22} are symmetric positive definite matrices with J_1 and J_2 defined in (17).

It follows from Lemma 1 that for the full column rank matrix $C^T \in \mathbb{R}^{n \times l}$, there exists the nonsingular matrix N such that $WC^T = C^T N$ holds. The inequality (16) is verified by the premultiplication and postmultiplication of (11) with Γ and Γ^T , respectively. The correlation matrices are constructed as follows:

$$\Gamma_1 = \text{Diag}\{\underbrace{P^{-1}, \dots, P^{-1}}_6, P_1^{-1}, I\}, \Gamma_2 = \text{Diag}\{P^{-1}, P^{-1}, P^{-1}\}, \Gamma = \text{Diag}\{\Gamma_1, \Gamma_2, \Gamma_2, \Gamma_2\}$$

Finally, solving the LMI (16) and the following equation (19) enables the determination of the extended state observer gain matrices Q , L and the controller gain matrix K within the co-design framework of FE and FTC.

$$Q = \tilde{Q}^T N^{-T}, L = \tilde{L}^T N^{-T}, K = \tilde{K}^T W^{-1} \quad (19)$$

The proof is completed.

4. SIMULATION

In this section, since the forward speed is the key parameter, simulations are conducted under two distinct scenarios: low speed and high speed of the USV. The parameters corresponding to the low-speed $V = 3.8$ m/s and high-speed $V = 7.8$ m/s configurations are delineated in Table 1. To align with practical scenarios and demonstrate the proposed algorithm's robustness to initial condition deviations, the initial state of the USV is set as $x(0) = [0.8 \quad -0.5 \quad 0.5 \quad -0.5 \quad 0.6]^T$.

The system matrices A , B , E in (3) derived from the parameters in Table 1 are shown in Table 2. It is noteworthy that in both scenarios, the system matrix C and the fault coefficient matrix F in (2) are chosen to be the same. At the same time, C satisfies the full column rank condition in Assumption 2. The specific values of C and F are also shown in Table 2. According to Lemma 1, the correlation matrices with the singular value decomposition of the matrix C manifest as follows.

$$J_1 = [0.5000 \quad -0.4000 \quad -0.5000 \quad 0.5000 \quad -0.3000], N = 1, \\ J_2 = \begin{bmatrix} 0.4000 & 0.8933 & -0.1333 & 0.1333 & -0.0800 \\ 0.5000 & -0.1333 & 0.8333 & 0.1667 & -0.1000 \\ -0.5000 & 0.1333 & 0.1667 & 0.8333 & 0.1000 \\ 0.3000 & -0.0800 & -0.1000 & 0.1000 & 0.9400 \end{bmatrix}, \Delta = 2. \quad (20)$$

Table 1. The relevant parameters of USV under the two scenarios [37]

Lowforwardspeed	Highforwardspeed
$T_v = 2/V, T_r = 1.6/V, K_{av} = 0.01V,$	$T_v = 1.8/V, T_r = 2/V, K_{av} = 0.06V,$
$K_{ar} = -0.0027V, K_{ap} = -0.0014V^2,$	$K_{ar} = -0.0036V, K_{ap} = -0.0022V^2,$
$K_{vp} = 0.21V, K_{vr} = -0.46 \text{ m/s},$	$K_{vp} = 0.16V, K_{vr} = -0.58 \text{ m/s},$
$\omega_n = 1.63 \text{ rad/s}, \zeta = 0.64 + 0.38V$	$\omega_n = 2.2 \text{ rad/s}, \zeta = 0.58 + 0.67V$

Table 2. The system matrices of USV under the two scenarios

Low forward speed	High forward speed
$A = \begin{bmatrix} -1.9000 & 0 & 0 & 0 & 0 \\ -1.0925 & -2.3750 & 0 & 0 & 0 \\ 0 & 1.0000 & 0 & 0 & 0 \\ 2.1202 & 0 & 0 & -6.7938 & -2.6569 \\ 0 & 0 & 0 & 1.0000 & 0 \end{bmatrix}$	$A = \begin{bmatrix} -4.3333 & 0 & 0 & 0 & 0 \\ -2.2620 & -3.9000 & 0 & 0 & 0 \\ 0 & 1.0000 & 0 & 0 & 0 \\ 6.0403 & 0 & 0 & -25.5464 & -4.8400 \\ 0 & 0 & 0 & 1.0000 & 0 \end{bmatrix}$
$B = \begin{bmatrix} 0.0722 & -0.0244 & 0 & -0.0537 & 0 \end{bmatrix}^T$	$B = \begin{bmatrix} 2.0280 & -0.1095 & 0 & -0.6478 & 0 \end{bmatrix}^T$
$C = \begin{bmatrix} 1 & 0.8 & 1 & -1 & 0.6 \end{bmatrix}$	$C = \begin{bmatrix} 1 & 0.8 & 1 & -1 & 0.6 \end{bmatrix}$
$E = \begin{bmatrix} 0 & 2.3750 & 0 & 0 & 0 \\ 0 & 0 & 0 & 2.6569 & 0 \end{bmatrix}^T$	$E = \begin{bmatrix} 0 & 3.9000 & 0 & 0 & 0 \\ 0 & 0 & 0 & 4.8400 & 0 \end{bmatrix}^T$
$F = \begin{bmatrix} 0.6 & -1 & 2 & 0.8 & 1 \end{bmatrix}^T$	$F = \begin{bmatrix} 0.6 & -1 & 2 & 0.8 & 1 \end{bmatrix}^T$

The disturbances are selected as $\omega_\psi(t) = \omega_1(t)0.9s/(s^2 + 2.2s + 1)$ and $\omega_\phi(t) = 0.15\cos(t)$, where ω_1 represent a vector of zero-mean Gaussian white noises. The upper bound of the delays on the SO and OC channels is selected as $\beta_M = 0.2, \sigma_M = 0.1, \theta_M = 0.15$. For Bernoulli deception attacks on the OC channel, the probability is set to $\bar{\rho} = 0.3$ and a smooth nonlinear function $\tanh(\cdot)$ is introduced to characterize the attacks. The specific forms of the deception attacks are as follows.

$$\mathfrak{N}(\hat{f}(t)) = -\tanh(0.2\hat{f}(t)), \mathfrak{N}(\hat{x}(t)) = \begin{pmatrix} -\tanh(0.3\hat{x}_1(t)) \\ -\tanh(0.6\hat{x}_2(t)) \\ -\tanh(0.5\hat{x}_3(t)) \\ -\tanh(0.4\hat{x}_4(t)) \\ -\tanh(0.8\hat{x}_5(t)) \end{pmatrix} \tag{21}$$

According to Theorem 2, the relevant parameters given are set as $\gamma = 1.2, \epsilon_1 = 0.6, \epsilon_2 = 1.8, \epsilon_3 = 0.9, \epsilon_4 = 1.8$. The gain matrices L and Q of the observer and the gain matrices K and G of the controller are obtained by solving inequality 16 and equation 19, as shown in Table 3.

To assess the efficacy of the algorithm when the USV faces the above multiple cyber-physical threats, four comparative simulation cases under two scenarios are given. In all subsequent experiments, the units of the components of the state vector $x(t)$ are $v(t) (m/s), r(t) (rad/s), \psi(t) (rad), p(t) (rad/s)$ and $\phi(t) (rad)$.

Case 1: In this situation, the USV is solely considered to face pure physical threats such as noise-type faults and disturbances. The specific form of noise-type fault is as follows. The state response $x(t)$ of the USV under noise-type actuator faults and disturbances is illustrated in Figure 3. Upon observation of the Figure 3, it is evident that the USV under the high-speed condition is significantly affected by disturbances and noise-type faults, resulting in a longer time for the system to achieve asymptotic stability compared to the low-speed condition. Nevertheless, across both low- and high-speed scenarios, the curves converge to bounded within a certain period of time, which verifies the effectiveness of the proposed algorithm in USV against physical threats.

Table 3. The correlation gain matrices of FE and FTC co-design under the two scenarios

Low forward speed	High forward speed
$Q = 0.65, G = 1.35$	$Q = 0.35, G = 1.05$
$L = \begin{bmatrix} -3.1626 & -1.5543 & 0.9668 & 0.9255 & -2.3214 \end{bmatrix}^T$	$L = \begin{bmatrix} -3.1530 & -1.0647 & 0.7674 & 1.0257 & -2.5214 \end{bmatrix}^T$
$K = \begin{bmatrix} 0.3642 & -1.3235 & 1.5725 & 0.4126 & 1.2125 \end{bmatrix}$	$K = \begin{bmatrix} 0.2642 & -1.2325 & 2.1125 & 0.3924 & 1.1225 \end{bmatrix}$

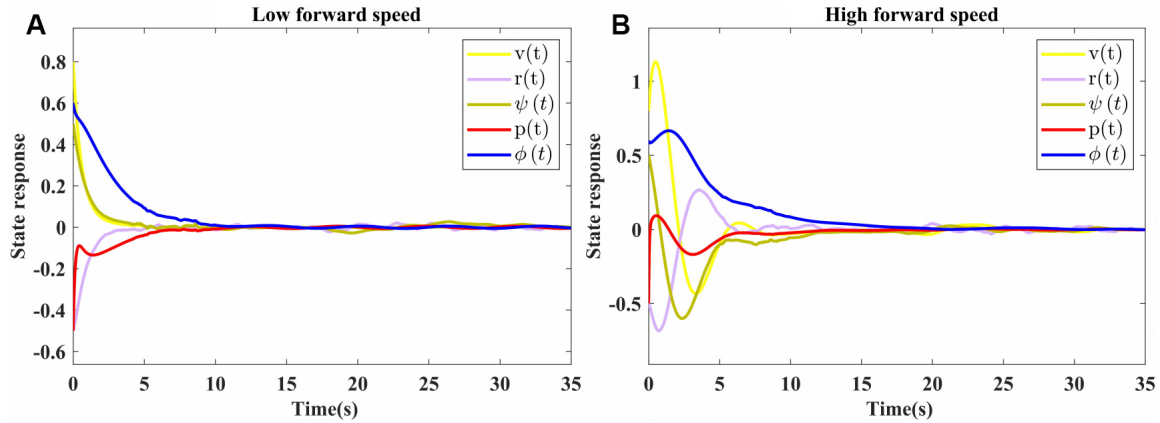


Figure 3. The state response $x(t)$ to disturbances and noise-type faults under two scenarios.

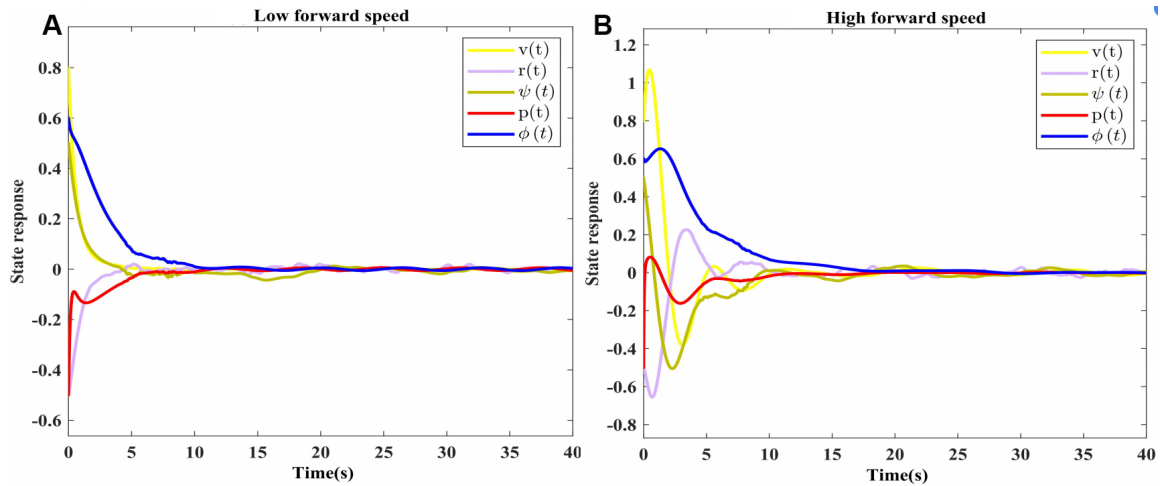


Figure 4. The state response $x(t)$ to noise-type actuator faults, disturbances, time-varying delays and constant injection attacks under two scenarios.

$$f(t) = \begin{cases} 0.3\omega_1(t)\sin(t), & t \in [4s, 10s] \\ 0, & \text{otherwise} \end{cases} \quad (22)$$

Case 2: This case is based on Case 1 to verify the effectiveness of the algorithm in the case of constant injection attacks and time-varying delays occurring within SO channel. The state response $x(t)$ of the USV under noise-type actuator faults, disturbances, time-varying delays and constant injection attacks is illustrated in Figure 4. Figure 4 shows that the curve fluctuates more frequently when the SO channel suffers from time-varying delays and constant injection attacks, but even under the high-speed scenario, the state response $x(t)$ still starts to stabilize at about 20s under the influence of the proposed algorithm.

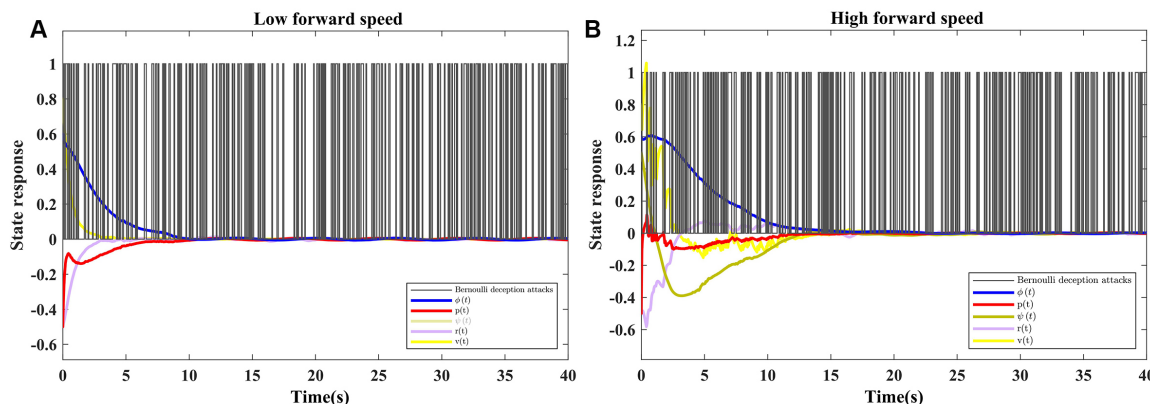


Figure 5. The state response $x(t)$ to noise-type actuator faults, disturbances, and dual-channel asynchronous injection and deception attacks under two scenarios.

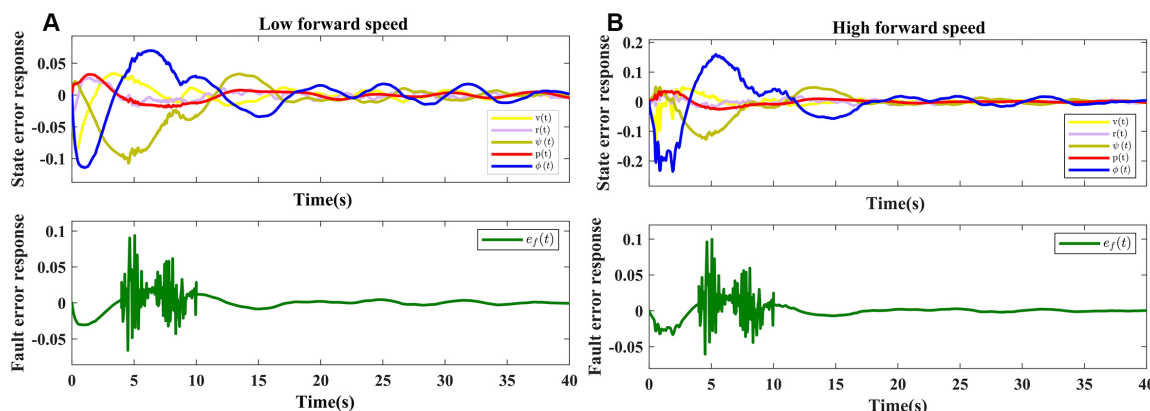


Figure 6. The state error response $e_x(t)$ and the fault error response $e_f(t)$ to noise-type actuator faults, disturbances, and dual-channel asynchronous injection and deception attacks under two scenarios.

Case 3: Based on Case 2, this case considers the existence of Bernoulli deception attacks and time-varying delays on OC channel, thus forming dual-channel asynchronous independent injection and deception attacks. [Figure 5](#) illustrates the trend of the state $x(t)$ of the USV in the face of multiple cyber-physical threats (noise-type actuator faults, disturbances, dual-channel asynchronous independent injection and deception attacks) under the two scenarios. It can be seen from [Figure 5](#) that even though Bernoulli deception attacks occur frequently, the state of the USV tends to be stable quickly and fluctuates less under both low- and high-speed scenarios, which verifies the feasibility of the proposed algorithm. [Figure 6](#) illustrates the state estimation error $e_x(t)$ and FE error $e_f(t)$ of the USV under the two scenarios, respectively. It can be seen from [Figure 6](#) that both the state estimation error $e_x(t)$ and the FE error $e_f(t)$ only fluctuate within a small range regardless of the low or high speed, even with many influences, thus demonstrating the good performance of the extended state observer proposed in this paper. [Figure 7](#) illustrates the variation in the control input response $u(t)$ of the USV under the specified physical threat scenario. It is observed that as the USV’s state reaches stabilization, the control input progressively stabilizes. It is noteworthy that the inclusion of disturbances and integrators within the simulation framework leads to the generation of FE even in the absence of actual faults.

Case 4: In this situation, firstly, the noise-type actuator faults in case 3 are replaced with stuck steering mechanism-type faults. [Figure 8](#) and [Figure 9](#) show the state response $x(t)$ and the error response $e_x(t)$ and $e_f(t)$ under the influence of stuck steering mechanism-type faults, disturbance, dual-channel asynchronous constant injection and Bernoulli deception attacks, respectively. Compared with the noise-type faults in Case

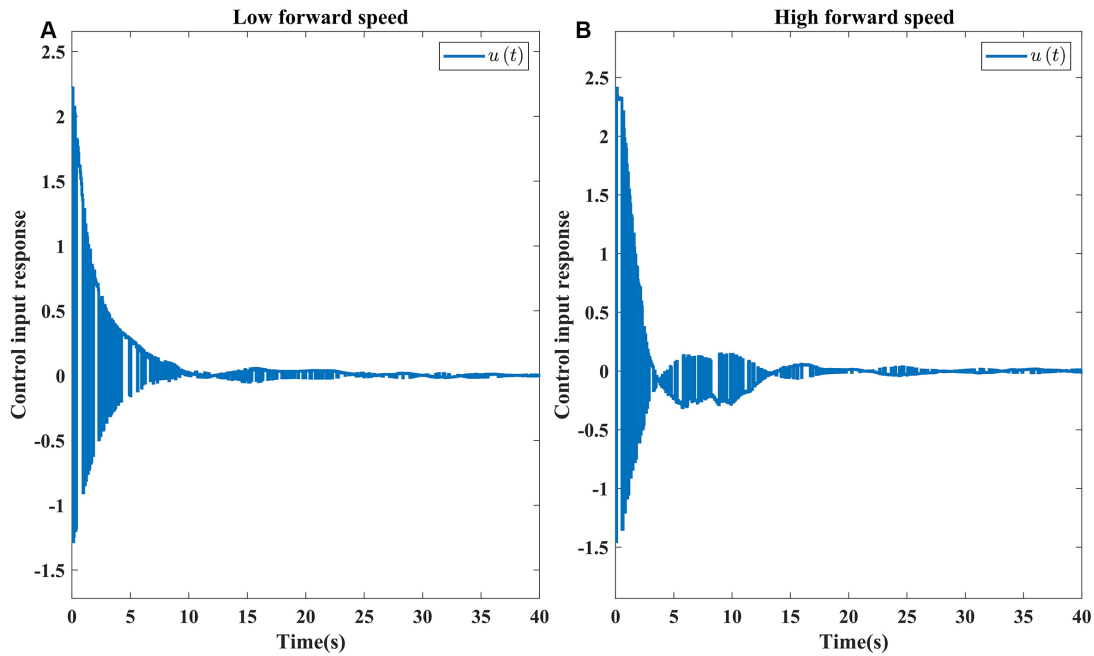


Figure 7. The control input response $u(t)$ under two scenarios.

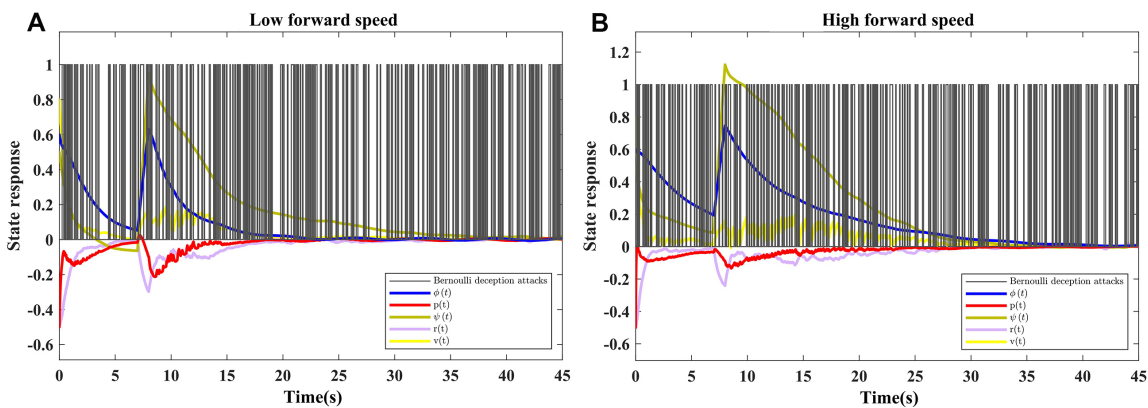


Figure 8. The error response $x(t)$ to stuck steering mechanism-type faults, disturbances, and dual-channel asynchronous injection and deception attacks under two scenarios.

3, the abrupt change of the stuck steering mechanism-type faults makes the stability of the USV more difficult, but the algorithm proposed in this paper still makes the USV tend to be stable in a certain period of time under the two scenarios. At the same time, the stuck steering mechanism-type faults also make the convergence of estimation error become relatively slow in the high-speed scenario. Secondly, in order to better characterize the impact of injection attacks, the constant injection attacks are replaced by time-varying or adaptive injection attacks. The specific forms of the stuck steering mechanism-type faults and the two types of injection attacks are as follows. It can be seen from Figure 10 and Figure 11 that the existence of time-varying injection attacks makes the state response $x(t)$ and error responses $e_x(t)$ and $e_f(t)$ fluctuate more sharply, but these fluctuations are still maintained in a tolerable range. Figure 12 and Figure 13 show that the adopted FTC scheme based on the extended state observer performs well against the adaptive injection attack.

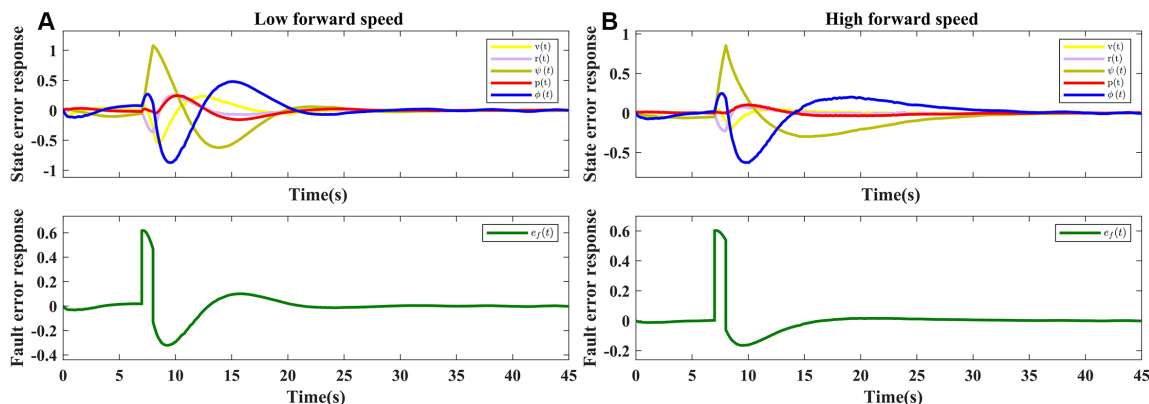


Figure 9. The error response $e_x(t)$ and $e_f(t)$ to stuck steering mechanism-type faults, disturbances, and dual-channel asynchronous injection and deception attacks under two scenarios.

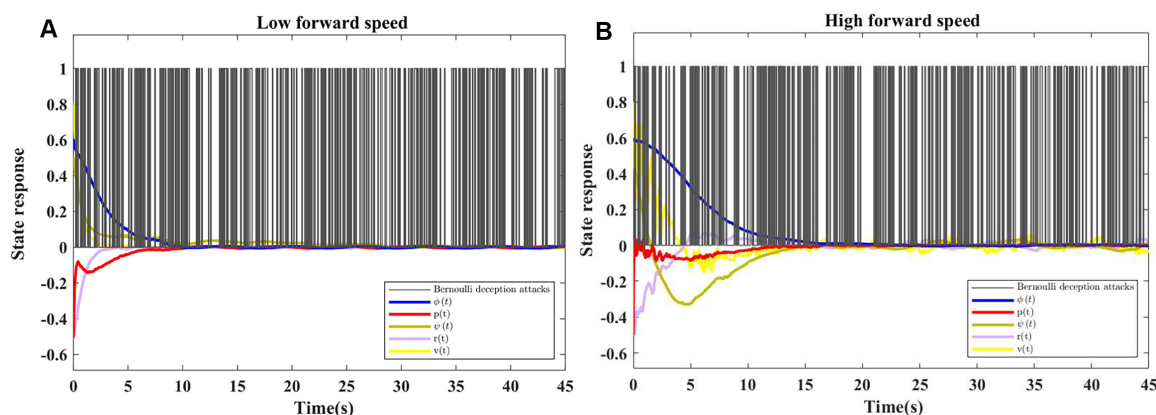


Figure 10. The state response $x(t)$ to noise-type faults, disturbances, and dual-channel asynchronous time-varying injection and deception attacks under two scenarios.

$$\begin{cases} \alpha = 0.1 \sin t \\ \dot{\alpha} = -2\alpha + 3\omega_2 \end{cases}, f(t) = \begin{cases} 0.6, & t \in [7s, 8s] \\ 0, & \text{otherwise} \end{cases} \quad (23)$$

where ω_2 is also a Gaussian white noise with variance 1.

5. CONCLUSIONS

A co-design method of FE and FTC for an underactuated USV under actuator faults, disturbances and cyber threats is proposed in this paper to achieve the smooth movement of the USV. To address the delays, uncertainties, and signal disruptions caused by dual-channel independent asynchronous injection and deception attacks, an extended state observer and a fault-tolerant controller were constructed using the compromised information, ensuring robust control of the USV under multiple cyber-physical threats. Utilizing the Lyapunov-Krasovskii functional, a sufficient condition for the integrated design was derived, and a method for eliminating equality constraints was proposed to overcome the challenges of solving nonlinear matrix inequalities. Simulation results validate the efficacy of the extended state observer-based FTC approach. This study advances theoretical foundations for the design of integrated FTC strategies and stability analysis of USVs under multi-layered adverse conditions. At the same time, it provides valuable insights for USVs to reliably navigate in modern complex network environments. Prospective research is encouraged to introduce the idea

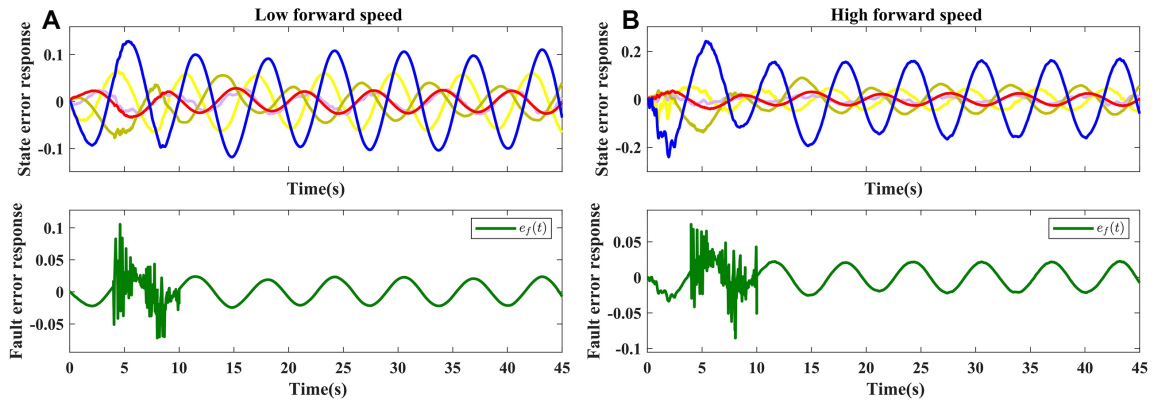


Figure 11. The error response $e_x(t)$ and $e_f(t)$ to noise-type faults, disturbances, and dual-channel asynchronous time-varying injection and deception attacks under two scenarios.

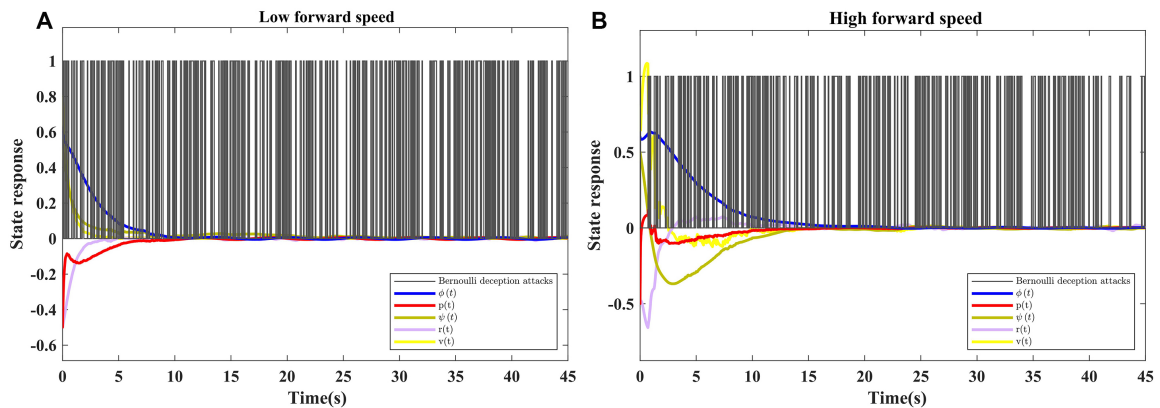


Figure 12. The state response $x(t)$ to noise-type faults, disturbances, and dual-channel asynchronous adaptive injection and deception attacks under two scenarios.

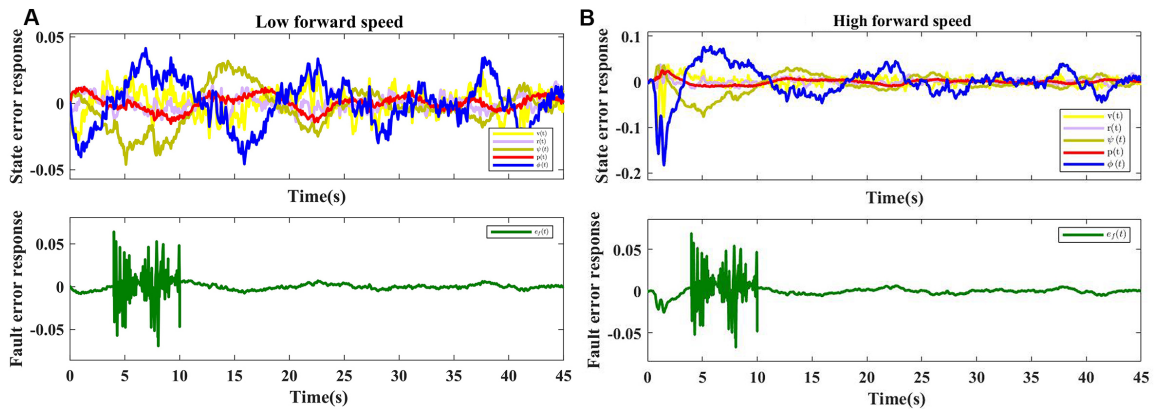


Figure 13. The error response $e_x(t)$ and $e_f(t)$ to noise-type faults, disturbances, and dual-channel asynchronous adaptive injection and deception attacks under two scenarios.

of the co-design into the cooperative control scenario of multi-USVs, aiming to enhance overall performance amidst the presence of diverse cyber-physical threats. In addition, insights from advanced control methods, such as reinforcement learning [38], can further enhance the adaptability of USVs in complex environments.

DECLARATIONS

Authors' contributions

Writing-original draft and conceptualization: Wang H, Liu C

Technical support: Huang X, Zhong Y, Qu D

Validation and supervision: Patton RJ

Availability of data and materials

Not applicable.

Financial support and sponsorship

This work was supported by the National Natural Science Foundation of China (62103250, 62273223, 62333011, and 62336005); Shanghai Sailing Program (21YF1414000); Project of Science and Technology Commission of Shanghai Municipality, China (22JC1401401); Joint Research Fund of Shanghai Academy of Spaceflight Technology (USCAST2023-22).

Conflicts of interest

Chun Liu and Ron J. Patton are the guest editors of the Special Issue of "Advancements in Fault-Tolerant Control and Security of Complex Systems", while the other authors have declared that they have no conflicts of interest.

Ethical approval and consent to participate

Not applicable.

Consent for publication

Not applicable.

Copyright

© The Author(s) 2024.

REFERENCES

1. Rao J, Xu X, Bian H, et al. A modified random network distillation algorithm and its application in USVs naval battle simulation. *Ocean Eng* 2022;261:112147. [DOI](#)
2. Rumson AG. The application of fully unmanned robotic systems for inspection of subsea pipelines. *Ocean Eng* 2021;235:109214. [DOI](#)
3. Wu J, Li R, Li J, Zou M, Huang Z. Cooperative unmanned surface vehicles and unmanned aerial vehicles platform as a tool for coastal monitoring activities. *Ocean Coastal Manage* 2023;232:106421. [DOI](#)
4. Er MJ, Ma C, Liu T, Gong H. Intelligent motion control of unmanned surface vehicles: a critical review. *Ocean Eng* 2023;280:114562. [DOI](#)
5. Zhang X, Xu X, Li J, et al. Observer-based fuzzy adaptive fault-tolerant control for NSC system of USV with sideslip angle and steering machine fault. *IEEE Trans Intell Veh* 2024;9:372-82. [DOI](#)
6. Meng X, Zhang G, Han B. Robust adaptive finite-time course tracking control of vessel under actuator attacks. *Complex Eng Syst* 2023;3:12 [DOI](#)
7. He S, Dai SL, Luo F. Asymptotic trajectory tracking control with guaranteed transient behavior for MSV with uncertain dynamics and external disturbances. *IEEE Trans Ind Electron* 2019;66:3712-20. [DOI](#)
8. Zhang G, Chu S, Zhang W, Liu C. Adaptive neural fault-tolerant control for USV with the output-based triggering approach. *IEEE Trans Veh Technol* 2022;71:6948-57. [DOI](#)
9. Yu XN, Hao LY. Integral sliding mode fault tolerant control for unmanned surface vessels with quantization: less iterations. *Ocean Eng* 2022;260:111820. [DOI](#)
10. Wu W, Li Y, Tong S. Neural network output-feedback consensus fault-tolerant control for nonlinear multiagent systems with intermittent actuator faults. *IEEE Trans Neural Netw Learn Syst* 2023;34:4728-40. [DOI](#)
11. Zhao XQ, Guo S, Long Y, Zhong GX. Simultaneous fault detection and control for discrete-time switched systems under relaxed persistent dwell time switching. *Appl Math Comput* 2022;412:126585. [DOI](#)
12. Li JN, Feng H, Wang Y, Liu GY. A novel failure-distribution-dependent non-fragile H_∞ fault-tolerant load frequency control for faulty multi-area power systems. *IEEE Trans Power Syst* 2024;39:2936-46. [DOI](#)
13. Zhou Z, Zhong M, Wang Y. Fault diagnosis observer and fault-tolerant control design for unmanned surface vehicles in network environ-

- ments. *IEEE Access* 2019;7:173694-702. DOI
14. Wang N, Deng Z. Finite-time fault estimator based fault-tolerance control for a surface vehicle with input saturations. *IEEE Trans Ind Inform* 2020;16:1172-81. DOI
 15. Li K, Feng K, Li Y. Fuzzy adaptive fault-tolerant formation control for USVs with intermittent actuator faults. *IEEE Trans Intell Veh* 2024;1-10. DOI
 16. Wan L, Cao Y, Sun Y, Qin H. Fault-tolerant trajectory tracking control for unmanned surface vehicle with actuator faults based on a fast fixed-time system. *ISA Trans* 2022;130:79-91. DOI
 17. Li J, Zhang G, Zhang X, Zhang W. Integrating dynamic event-triggered and sensor-tolerant control: application to USV-UAVs cooperative formation system for maritime parallel search. *IEEE Trans Intell Transp Syst* 2023;1-13. DOI
 18. Hao LY, Yu Y, Li TS, Li H. Quantized output-feedback control for unmanned marine vehicles with thruster faults via sliding-mode technique. *IEEE Trans Cybern* 2022;52:9363-76. DOI
 19. Zhang G, Liu S, Zhang X. Adaptive distributed fault-tolerant control for underactuated surface vehicles with bridge-to-bridge event-triggered mechanism. *Ocean Eng* 2022;262:112205. DOI
 20. Meng X, Zhang G, Han B. Fault-tolerant control of underactuated MSVs based on neural finite-time disturbance observer: an event-triggered mechanism. *J Frankl Inst Eng Appl Math* 2024;361:106603. DOI
 21. Liu Q, Cai Z, Chen J, Jiang B. Observer-based integral sliding mode control of nonlinear systems with application to single-link flexible joint robotics. *Complex Eng Syst* 2021;1:8 DOI
 22. Zeng H, Su Z, Xu Q, Li R. Security and privacy in space-air-ocean integrated unmanned surface vehicle networks. *IEEE Netw* 2024;38:48-56. DOI
 23. Liu C, Jiang B, Wang X, Zhang Y, Xie S. Event-based distributed secure control of unmanned surface vehicles with DoS attacks. *IEEE Trans Syst Man Cybern Syst* 2024;54:2159-70. DOI
 24. Ma Y, Nie Z, Hu S, et al. Fault detection filter and controller co-design for unmanned surface vehicles under DoS attacks. *IEEE Trans Intell Transp Syst* 2021;22:1422-34. DOI
 25. Liu C, Xia Z, Tian Y, Patton RJ. Defense and tolerance technique against attacks and faults on leader-following multi-USVs. *IEEE Trans Intell Transp Syst* 2024;25:5450-61. DOI
 26. Zhang D, Ye Z, Feng G, Li H. Intelligent event-based fuzzy dynamic positioning control of nonlinear unmanned marine vehicles under DoS attack. *IEEE Trans Cybern* 2022;52:13486-99. DOI
 27. Gao S, Peng Z, Liu L, Wang H, Wang D. Coordinated target tracking by multiple unmanned surface vehicles with communication delays based on a distributed event-triggered extended state observer. *Ocean Eng* 2021;227:108283. DOI
 28. Lei T, Wen Y, Yu Y, Tian K, Zhu M. Predictive trajectory tracking control for the USV in networked environments with communication constraints. *Ocean Eng* 2024;298:117185. DOI
 29. Nemati A, Peimani M, Mobayen S, Sayyedfatahi S. Adaptive non-singular finite time control of nonlinear disturbed cyber-physical systems with actuator cyber-attacks and time-varying delays. *Inf Sci* 2022;612:1111-26. DOI
 30. Fei Z, Wang X, Wang Z. Event-based fault detection for unmanned surface vehicles subject to denial-of-service attacks. *IEEE Trans Syst Man Cybern Syst* 2022;52:3326-36. DOI
 31. Wu C, Zhu G, Lu J. Indirect adaptive neural tracking control of USVs under injection and deception attacks. *Ocean Eng* 2023;270:113641. DOI
 32. Yin T, Gu Z, Park JH. Event-based intermittent formation control of multi-UAV systems under deception attacks. *IEEE Trans Neural Netw Learn Syst* 2024;35:8336-47. DOI
 33. Liu ZQ, Ge X, Han QL, Wang YL, Zhang XM. Secure cooperative path following of autonomous surface vehicles under cyber and physical attacks. *IEEE Trans Intell Veh* 2023;8:3680-91. DOI
 34. Zhao D, Tian Y, Zhao N. Adaptive neural control for delayed discrete-time switched systems under deception attacks. *Complex Eng Syst* 2024;4:1 DOI
 35. Wang D, Chen F, Meng B, Hu X, Wang J. Event-based secure ∞ load frequency control for delayed power systems subject to deception attacks. *Appl Math Comput* 2021;394:125788. DOI
 36. Dai S, Zha L, Liu J, Xie X, Tian E. Fault detection filter design for networked systems with cyber attacks. *Appl Math Comput* 2022;412:126593. DOI
 37. Wang YL, Han QL. Network-based fault detection filter and controller coordinated design for unmanned surface vehicles in network environments. *IEEE Trans Ind Inform* 2016;12:1753-65. DOI
 38. Bai W. Introduction to discrete-time reinforcement learning control in Complex Engineering Systems. *Complex Eng Syst* 2024;4:8 DOI